Mapping water exchange in rat tumour xenografts: using multiple flip angles during late-uptake stages following contrast agent injection

Colleen Bailey[1,2], Firas Moosvi[1,2], and Greg J Stanisz[1,2]
[1]*Medical Biophysics, University of Toronto, Toronto, ON, Canada,* [2]*Imaging Research, Sunnybrook Health Sciences Centre, Toronto, ON, Canada*

INTRODUCTION: Water exchange from the intracellular to extracellular space (ECS) increases following induction of apoptotic cell death in vitro (1), showing promise for monitoring cancer therapy. Work in vivo is complicated since quantitative assessment of exchange requires knowledge of the contrast agent concentration. Previous methods have made use of a constant infusion where large numbers of points on the T1 recovery curve can be obtained (2), but this method is time-consuming due to the time needed to adjust concentrations. Other work has focussed on adapting dynamic contrast-enhanced MRI (DCE-MRI) techniques by adding measurements at two new flip angles in the late stages following injection (3), where contrast agent concentration does not vary significantly, limiting the concentration range these two flip angles probe. This work uses T1 data at four flip angles in the late-uptake stages following three separate injections of contrast agent to determine water exchange rate in a rat tumour xenograft.

METHODS: Five female nude rats (6-8 weeks) were implanted with ~5 million MDA-MB-231 cells subcutaneously in the hind limb. Tumours were grown for ~6 weeks until they reached a diameter of 1-2 cm. Rats underwent three bolus injections: (i) 0.1 mL Gd-DTPA-BMA (Omniscan, GE Healthcare, Milwaukee, WI) diluted to 0.3 mL with saline, (ii) 0.2 mL Gd-DTPA-BMA diluted to 0.3 mL with saline and (iii) 0.3 mL Gd-DTPA-BMA.

MRI: Animals were scanned at 7 T (Bruker Biospin, Germany) with a 2 cm receiver surface coil. All images were 3 x 4 cm^2 field of view with 1 mm slice thickness and a saturation band across the body to limit motion artefact and signal from blood. Uptake following injection was monitored with a 3D SPGR-based DCE sequence (64 x 96 x 8 matrices, flip angle α=16.6-20°, repetition time TR=20 ms, echo time TE=2.5 ms, temporal resolution 10.2 s) until it appeared constant in the tumour rim. During this steady-state, 3D SPGR sequences (128 x 96 x 8 matrices; TR=20 ms; TE=2.5 ms) at four flip angles (α=16.6-20, 11, 7 and 5°) were performed. These four SPGRs were also run prior to injection, along with a 2D inversion recovery (IR) sequence (64 x 96 matrices; inversion time TI=62.1, 100, 300, 700, 900, 1200 and 1500 ms; TR=2500 ms; TE=11.6 ms) to correct for B1 inhomogeneities.

Analysis: Data from all four Gd-DTPA-BMA concentrations at all four flip angles were fit globally to a two-compartment model of relaxation incorporating exchange, as described by the modified Bloch equations in (4). This gives four free fit parameters: equilibrium signal S_0, intracellular longitudinal relaxation time $T1_I$, extracellular water fraction M_{0E}, and water exchange from the intracellular to extracellular space k_{IE}. Relaxation of water in the extracellular space is given by $\frac{1}{T1_E} = \frac{1}{T1_{E0}} + r_1 C_{ECS}$, where $T1_{E0}$ is the extracellular relaxation in the absence of Gd-DTPA-BMA, fixed to 1.5 s; r_1=4.2 $mM^{-1}s^{-1}$ is the relaxivity at 7 T and C_{ECS} is the concentration of Gd-DTPA-BMA in the ECS. At steady-state, $C_{ECS}=C_p$, the concentration in blood plasma and is assumed to be equal to the amount of Gd-DTPA-BMA injected divided by 20% of the rat's weight (ie. the distribution volume is assumed to be 20%): $C_p = \frac{V_{Gd} C_{inj}}{0.2 m_{rat}}$ [1]. Clearance by the kidneys was assumed to be negligible over the course of the experiment (~20 mins). Statistical errors in the exchange rate parameter were determined at the 68% confidence level as described in (5). Only values that were reliably fast (Lower bound > 2 s^{-1}) or well-determined (Upper bound < 5 s^{-1}) are included in the parametric maps. Regions that were not in steady-state based on the DCE scans were also excluded.

Histology: After scanning, three tumours were frozen in OCT gel at -80°C and two were fixed in formalin. Levels were cut 1 mm apart and an H&E-stained slice and a TUNEL-stained slice were obtained at each level. Slides were scanned with a Mirax scanner (Carl Zeiss MicroImaging, Göttingen) and aligned manually with MRI.

RESULTS: Parametric maps of extracellular water fraction, M_{0E}, and water exchange rate, k_{IE}, in three rats are overlaid on the final contrast-enhanced image in the first two columns of Figure 1. Equilibrium signal, S_0, and intracellular water fraction, $T1_I$, (not shown) show little variation. H&E and TUNEL staining are presented in the last two columns of Figure 1. Figure 2 shows a close-up of an area including two regions (arrows) where small patches of apoptosis are apparent on TUNEL, but cells have not yet been cleared away. Extracellular water fraction is still low in this area, while exchange is high.

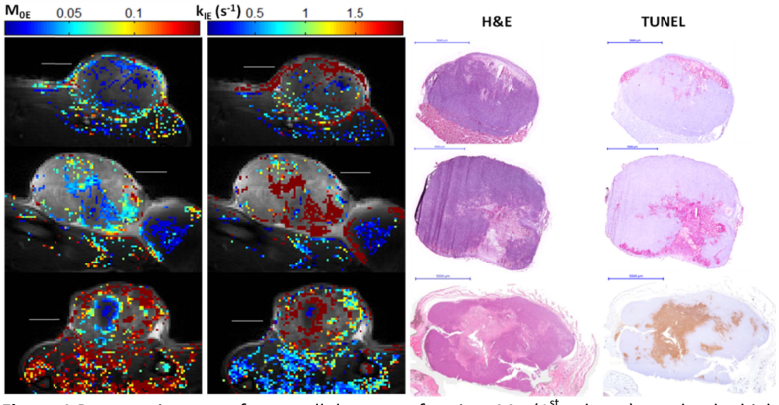

Figure 1 Parametric maps of extracellular water fraction, M_{0E} (1st column), tend to be higher where dead cells have been cleared to leave more extracellular space (lighter areas on H&E, 3rd column). Maps of water exchange, k_{IE} (2nd column), are higher in areas that are apoptotic on TUNEL (last column), even when M_{0E} remains low (see Fig. 2). Scale bars indicate 5 mm.

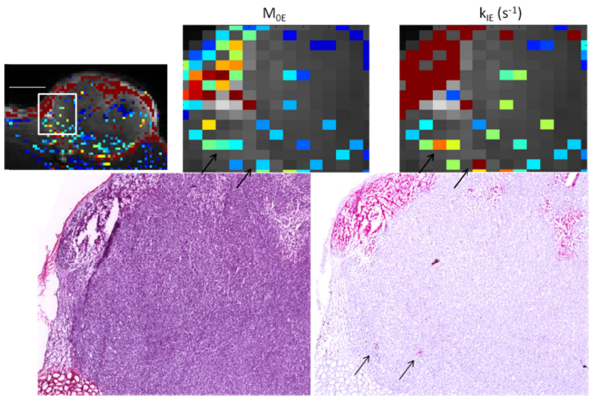

Figure 2 Close-up of the first tumour for the area shown in the white box at the top left of the figure. Two apoptotic regions, shown by the arrows, where there is not yet cell clearance and M_{0E} remains low, have increased k_{IE}.

DISCUSSION: The use of Eq. 1 to determine C_p is based on previous pharamcokinetic studies in these rats, but has some error associated with it. It would be preferable to measure the Gd-DTPA-BMA concentration in the blood, but this was not possible with the current data given the small vessel size in rats. The assumption that M_{0E} is inversely proportional to rat weight mainly affects the absolute value of M_{0E}; relative values of M_{0E} in a given animal can still be compared in these maps since the concentration of Gd-DTPA-BMA is the same everywhere in the ECS at steady-state and a poor assumption about its value will result in the same error for each voxel. The exchange rate is subject to error from the assumption that clearance is negligible. However, the DCE monitoring curves showed little difference in signal intensity between the end of one injection and the start of the next, when steady-state scans were run. It should also be noted that the values seen here in the muscle (~0.5-0.8 s^{-1}) are comparable to those obtained in other studies (2), suggesting the clearance assumption is reasonable. As with previous similar studies (2,3), the precision of exchange was low in many cases (wide range in statistical error bounds), particularly when cellularity was high and overall concentration of Gd-DTPA-BMA in the tumour was low. These wide error ranges and the steady-state requirement limit the tumour types and regions (such as the uncoloured spaces in Fig. 1 above) where this model can be applied. However, in cases where the model can be applied, regions of high exchange correlate with TUNEL-positive regions, suggesting exchange can be used as a marker of apoptosis in vivo.

REFERENCES: 1. Bailey C, et al. (2009). Magn. Reson. Med. 62: 46-55. 2. Landis et al. (1999). Magn. Reson. Med. 42: 467-478. 3. Buckley et al. (2008). Magn. Reson. Med. 60: 1011-1019. 4. McConnell HM. (1958). J. Chem. Phys. 28: 430-431. 5. Stanisz GJ, et al. (1999). Magn. Reson. Med. 42: 1128-1136.